

Atomically Resolved Observations of Antiphase Domain Boundaries in Epitaxial Fe_3O_4 Films on $\text{MgO}(001)$ by Scanning Tunneling Microscopy

To cite this article: Akira Ikeuchi *et al* 2012 *Jpn. J. Appl. Phys.* **51** 08KB02

View the [article online](#) for updates and enhancements.

You may also like

- [Evolution of quadrupole-octupole collectivity in the even-even 54 \$Z\$ 58 nuclei](#)
Nikolay Minkov
- [Role of anti-phase boundaries in the formation of magnetic domains in magnetite thin films](#)
Roberto Moreno, Sarah Jenkins, Aleksandar Skeparovski *et al.*
- [From surface data to bulk properties: a case study for antiphase boundaries in GaP on Si\(001\)](#)
P Farin, H Eisele, M Dähne *et al.*

Atomically Resolved Observations of Antiphase Domain Boundaries in Epitaxial Fe₃O₄ Films on MgO(001) by Scanning Tunneling Microscopy

Akira Ikeuchi*, Satoshi Hiura, Taichi Mizuno, Eisaku Kaji, Agus Subagyo, and Kazuhisa Sueoka

Graduate School of Information Science and Technology, Hokkaido University, Sapporo 060-0814, Japan

Received January 15, 2012; revised February 20, 2012; accepted April 3, 2012; published online August 20, 2012

We have studied the surface atomic configurations around antiphase domain boundaries (APBs) in epitaxial magnetite (Fe₃O₄) thin films on MgO(001) by scanning tunneling microscopy (STM). The observed surface of the Fe₃O₄ films is the B-plane terminating surface with the $(\sqrt{2} \times \sqrt{2})R45^\circ$ reconstruction. Several variations of APBs are observed by STM at atomic resolution. The observed APBs are categorized into a APBs labeled by three different phase shift vectors: in-plane 1/4[110], in-plane 1/2[100], and out-of-plane 1/4[101]. We discussed how these APBs appear on the surface. The proportions of the APBs with 1/4[110], 1/2[100], and 1/4[101] shifts are about 38, 1, and 61%, respectively, in our experiment. © 2012 The Japan Society of Applied Physics

1. Introduction

Magnetite (Fe₃O₄) has been attracting much attention because of its electrical and magnetic properties such as half-metallicity and a high Curie temperature of 858 K.^{1–3)} From the viewpoint of its application to spin-related devices, thin films of Fe₃O₄ are also interesting because they have fascinating potential properties that could provide highly spin-polarized electrodes for such devices. However, Fe₃O₄ films grown epitaxially on MgO substrates (MgO is an insulating material often used in spin-sensitive devices) contain a high density of antiphase domain boundaries (APBs).^{4–6)} These APBs make the electrical and magnetic properties of the films complicated. For example, APB-induced magnetic domains as small as 5 to 10 nm were studied by Lorentz microscopy.⁷⁾ The atomic configurations of APBs in an epitaxial Fe₃O₄(110) films and its effects on their magnetic properties have been discussed.⁸⁾ In addition to these reports, it has recently been reported that APBs can induce inhomogeneous electronic properties on the surface of Fe₃O₄(001).⁹⁾ Therefore, it would also be interesting to study the effects of APBs on surface electronic states as well as on magnetic properties.

APBs with seven different shift vectors can exist in epitaxial Fe₃O₄ layers.⁵⁾ Seven different types of APBs in the bulk films have been observed, and the atomic configurations of the APBs have been discussed.⁶⁾ However, there have been no reports yet on the surface atomic configurations of APBs in the film surface of Fe₃O₄(001). We have used scanning tunneling microscopy (STM) to identify the atomic structures of the APBs. In this paper, we report STM studies of epitaxial Fe₃O₄ films on MgO(001) and reveal the surface atomic configurations around APBs.

2. Experimental Procedure

The experiments were performed in an ultrahigh-vacuum (UHV) system consisting of a chamber for Fe₃O₄ film growth and a chamber for STM. The base pressure of both chambers was 2.0×10^{-10} mbar. STM was performed at room temperature with W tips. The W tips were made of a polycrystalline W wire electrochemically etched in 4M NaOH solution. The tips were cleaned by electron beam heating in the UHV. STM images were acquired in a

constant-current mode. The bias voltage was applied to the sample with respect to the grounded tip.

Epitaxial Fe₃O₄(001) films were prepared on mechanically polished MgO(001) single-crystal substrates by the deposition of Fe at 523 K in the presence of oxygen. The MgO(001) substrates were cleaned *in situ* by heating at 523 K for 16 h and then annealed at 1073 K for 1 h in oxygen atmosphere (7×10^{-7} mbar). Fe was evaporated from high-purity Fe rods heated by electron bombardment. The growth rate was 1.5 ML/min and the film thickness was 20 nm.¹⁰⁾ The oxygen pressure was set in the range of 7.0×10^{-7} to 1.0×10^{-6} mbar. To obtain a flat surface, the as-grown films were annealed in oxygen atmosphere by keeping the temperature constant at 523 K for 30 min.¹⁰⁾

3. Results and Discussion

3.1 Surface termination

Bulk Fe₃O₄ has a cubic inverse spinel structure with a lattice constant of 8.397 Å.¹¹⁾ In the [001] direction, A layers of tetrahedral iron (Fe_A) and B layers containing oxygen and octahedral iron (Fe_B) are stacked alternately as shown in Fig. 1(a). A B-terminated surface with the $(\sqrt{2} \times \sqrt{2})R45^\circ$ reconstruction has often been observed on the Fe₃O₄(001) surface by STM.^{12–14)} Several models have been proposed to explain this reconstruction on the basis of the formation of Fe²⁺–Fe²⁺ and Fe³⁺–Fe³⁺ pairs along the Fe_B rows,¹³⁾ B layer termination with one oxygen vacancy per unit cell,^{14,15)} or Jahn–Teller distortion in the B-terminated surface.¹⁶⁾

An STM image of the epitaxially grown Fe₃O₄(001) surface is shown in Fig. 2(a). Atomically flat terraces can be seen. The minimum step height is ~ 0.21 nm, as revealed by the line profile shown in Fig. 2(b). This step height corresponds to the A–A or B–B layer separation distance of Fe₃O₄. It indicates that the surface is terminated at the A- or B-plane. Additionally, we show a high-resolution STM image in Fig. 3. Rows running along [110] can be clearly seen. The distance between two rows is ~ 0.6 nm, and the distance between two bright spots within the rows is ~ 0.3 nm. Since the periodicities of ~ 0.6 and ~ 0.3 nm correspond to those of Fe_B in the B-plane, each bright spot in the STM images should represent a single Fe_B. Therefore, we conclude that the surface is terminated by the B-plane. STM also resolved the $(\sqrt{2} \times \sqrt{2})R45^\circ$ reconstruction (indicated by the square in Fig. 3), which has been reported by several groups.^{12–14)}

*E-mail address: ikeuchi@nano.ist.hokudai.ac.jp

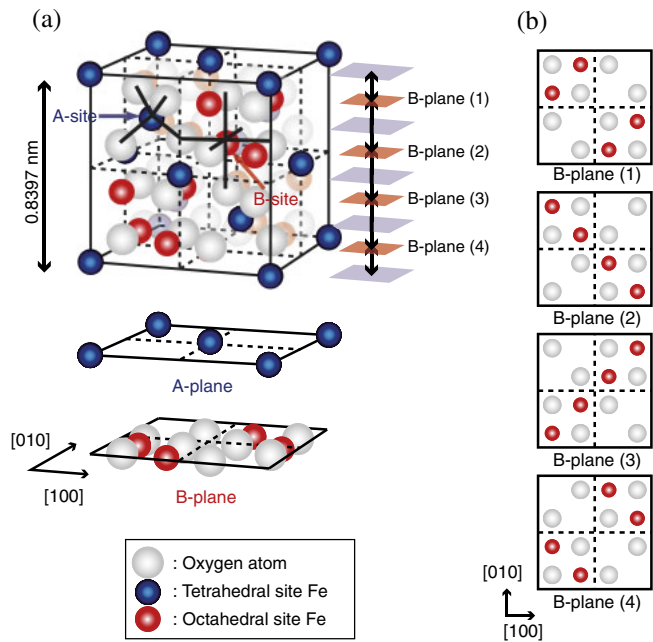


Fig. 1. (Color online) (a) Cubic inverse spinel structure of Fe_3O_4 . Tetrahedral iron (Fe_A) in the A-plane, a octahedral iron (Fe_B) in the B-plane, and oxygen are indicated by a reddish circle, a bluish circle, and a grayish circle, respectively. (b) Four possible types of surface unit cells in unrelaxed B-plane termination $\text{Fe}_3\text{O}_4(001)$ surfaces. Precise surface relaxation should be considered, and surface unit cells do not coincide with the actual unit cell on the surfaces. However, it is convenient to use these unit cells for understanding atomic arrangements around APBs.

3.2 Surface atomic configurations around APBs

The APBs are distinguished by seven different shift vectors.⁵⁾ The $1/4[110]$, $1/4[\bar{1}\bar{1}0]$, and $1/2[100]$ shifts ($1/4[101]$, $1/4[10\bar{1}]$, $1/4[011]$, and $1/4[01\bar{1}]$ shifts) are classified as in-plane shifts (out-of-plane shifts). The atomic structure of the $1/4[110]$ shift ($1/4[101]$ shift) is equivalent to that of the $1/4[\bar{1}\bar{1}0]$ shift ($1/4[10\bar{1}]$, $1/4[011]$, and $1/4[01\bar{1}]$ shifts). Therefore, here we describe only the $1/4[110]$, $1/2[100]$, and $1/4[101]$ shifts.

In this section, we discuss STM images of the Fe_3O_4 surface that includes APBs and investigate models of the atomic configurations around the APBs. Models of APBs in the bulk have been reported by Celotto *et al.*⁶⁾ In addition, it has been observed that the surface structure of Fe_B is not significantly different from the structure of Fe_B in the bulk.^{10,12,14)} Thus, we based the surface structure models of the APBs on the bulk configuration.

3.2.1 In-plane $1/4[110]$ shift

A topographic image of an APB observed on the surface of an epitaxial grown Fe_3O_4 film is shown in Fig. 4(a). Two domains are coreless and the APB has formed in between them, as indicated by a dashed line. As shown in this figure, APBs are observed as regions where the periodicity of the corrugation in the image is disrupted. According to the above assumption in which bright corrugation should be assigned to the location of the topmost Fe_B cations, the atomic arrangement of this surface could be represented by a model shown in Fig. 4(b). In this drawing, the topmost layer on the surface and the second layer in the subsurface are shown. Oxygen anions are represented by large circles.

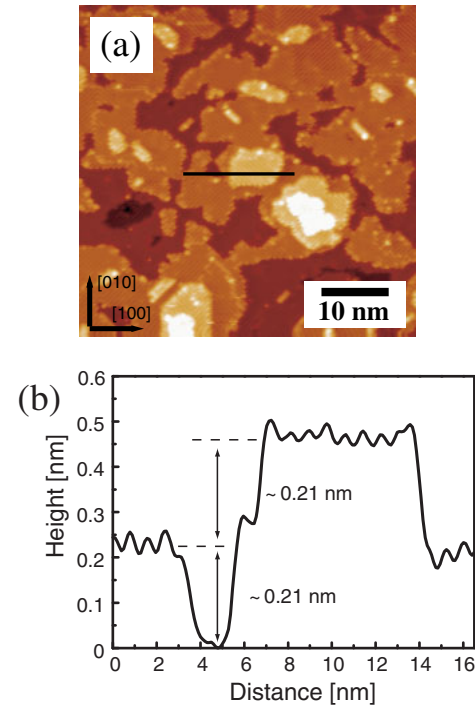


Fig. 2. (Color online) (a) STM image of Fe_3O_4 film on $\text{MgO}(001)$. The feedback control set point was $V_S = 2.0 \text{ V}$, $I = 1 \text{ nA}$. The scan size was $50 \times 50 \text{ nm}^2$. Atomically flat terraces exhibiting atomic rows oriented along the $[110]$ direction can be seen. (b) Line profile taken along the black line in the STM image. The step height of $\sim 0.21 \text{ nm}$ is indicated.

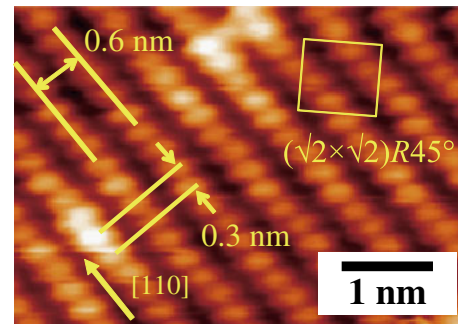


Fig. 3. (Color online) High-resolution STM image of Fe_3O_4 film on $\text{MgO}(001)$. The feedback control set point was $V_S = 2.0 \text{ V}$, $I = 1 \text{ nA}$. The scan width was 5 nm . The $(\sqrt{2} \times \sqrt{2})R45^\circ$ reconstruction unit cell is indicated by the yellow square.

Lighter circles (red online) indicate Fe cations in octahedral sites (B sites) on the topmost (001) surface and darker ones (blue online) are Fe cations in tetrahedral sites (A sites) located in the second layer. Around these lighter circles, topography observed by STM should be imaged as brighter regions. In the STM image shown in Fig. 4(a), single Fe_B sites are not resolved owing to the tip condition; however, bright rows running in the $[1\bar{1}0]$ direction are observed. The distance between two Fe_B rows on each domain is $\sim 0.6 \text{ nm}$ as indicated by black lines in Figs. 4(a) and 4(b). On the other hand, the distance between two Fe_B rows separated by the APB (indicated by gray lines, red online) is $\sim 0.9 \text{ nm}$. These features are explained using the APB with a $1/4[110]$ shift vector. As shown in Fig. 4(b), two domains indicated by hatched areas are grown on the

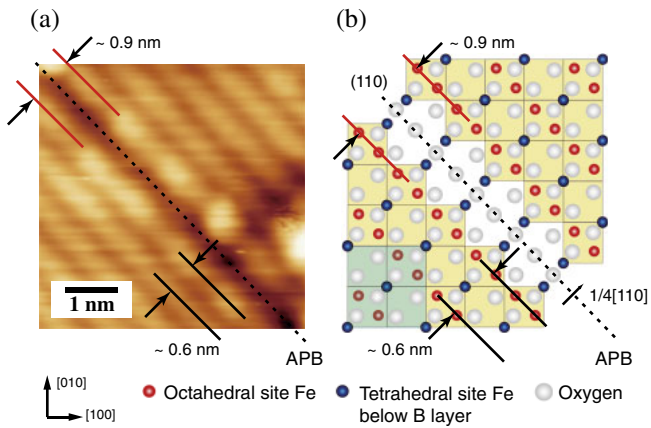


Fig. 4. (Color online) (a) STM image of an APB with a $1/4[110]$ shift. The feedback control set point was $V_S = 2.0$ V, $I = 0.3$ nA. The scan size was 5×5 nm². The APB is in a (110) plane. (b) Possible surface atomic configuration around an APB with a $1/4[110]$ shift.

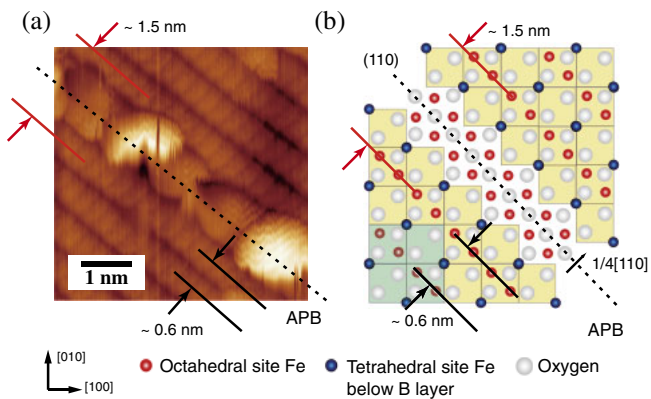


Fig. 5. (Color online) (a) STM image of an APB which has a $1/4[110]$ shift. The feedback control set point was $V_S = 1.5$ V, $I = 0.7$ nA. The scan size was 5×5 nm². (b) Possible surface atomic configuration around an APB with a $1/4[110]$ shift.

surface with a different phase of the periodicity characterized by the shift vector of $1/4[110]$. In the left bottom of this figure, a unit cell is marked to explain the origin of periodicity in the domains.

Since there are four types of B-plane in which Fe_B cations are aligned in two different directions with two different phases as shown in Fig. 1(b), the APBs with the $1/4[110]$ shift vector emerge on the surface in four different ways. By seeking several areas of the surface, two other means of the emergence have been found. Figure 5(a) shows an APB that divides domains. The domains have the topmost Fe cations aligned along the $[1\bar{1}0]$ direction as in the image shown in Fig. 4(a). The detailed structure of the APB is vague in the STM image, and it is not clear whether contaminants or instability of the structure causes this ambiguous image. However, the distance between two Fe_B rows separated by the APB is thought to be ~ 1.5 nm, and the atomic arrangement of the surface is shown in Fig. 5(b). The difference between Figs. 4(b) and 5(b) is due to the translational relations of the Fe_B rows observed in B-planes (4) and (2), as indicated in Fig. 1(b). For convenience, two proximate Fe_B cations are depicted in the region of the APB.

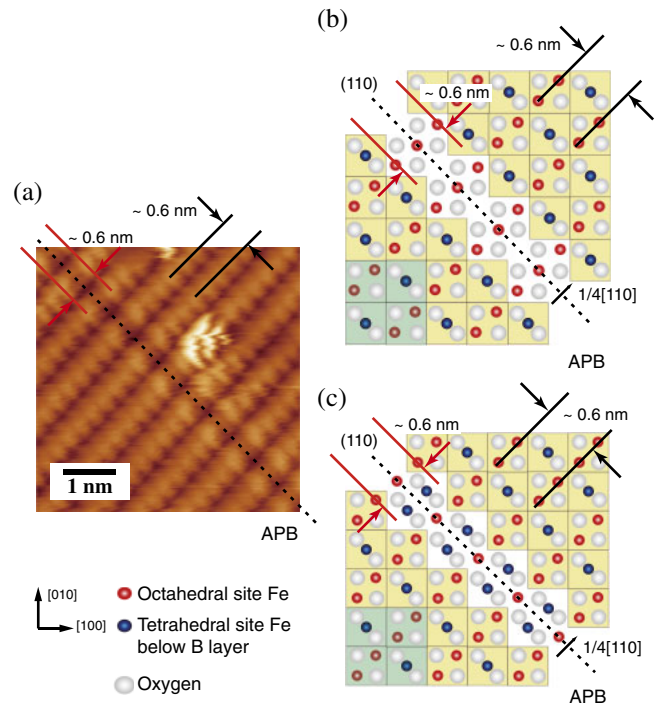


Fig. 6. (Color online) (a) STM image of an APB with a $1/4[110]$ shift. The feedback control set point was $V_S = 1.5$ V, $I = 0.8$ nA. The scan size was 5×5 nm². (b) and (c) Possible surface atomic configuration around an APB with a $1/4[110]$ shift.

However, it is difficult to discuss the atomic arrangement on the basis of this experimental result.

Figure 6(a) also shows an STM image of the APB characterized by the in-plane shift vector of $1/4[110]$. Fe_B rows running in the $[110]$ direction are divided by the APB. The APB is observed as a darker valley. The Fe_B cations beside the APB are imaged as slightly brighter spots, and the distance between the spots over the APB is ~ 0.6 nm. It should be considered that the observed APB is in B-plane (1) or (3), as shown in Fig. 6(b) or 6(c). The main difference between the models depicted in these figures is in the periodicity of the Fe_A cations. More detailed study of electronic states around the APB should be required to identify which model is preferable to understand the obtained STM image.

As discussed above, our experimental results indicate that the APBs with the in-plane $1/4[110]$ shift are observed in at least three different ways. This depends on which B-plane is exposed at the surface. According to the crystallographic structure of Fe_3O_4 , four different ways are observed for the APBs with the $1/4[110]$ shift.

3.2.2 In-plane $1/2[100]$ shift

An STM image of an APB described by an in-plane shift vector of $1/2[100]$ is shown in Fig. 7(a). As discussed in the previous section, four different types of B-planes should be considered. However, two of them form equivalent atomic arrangements because of the symmetry of the APB. That is, APBs in B-planes (1) and (3) or B-planes (2) and (4) have the same atomic pattern. In this STM image, bright rows corresponding to Fe_B cation rows run in the $[110]$ direction; they shift by ~ 0.3 nm at the APB. This APB is a region where two domains shifted by $1/2[100]$ coalesce, as shown

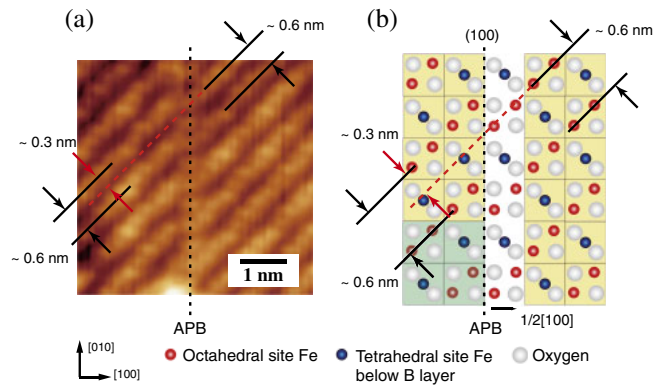


Fig. 7. (Color online) (a) STM image of an APB with a $1/2[100]$ shift. The feedback control set point was $V_S = 1.6$ V, $I = 1$ nA. The scan size was 5×5 nm². The APB is in a (100) plane. (b) Possible surface atomic configuration around an APB with a $1/2[100]$ shift.

in Fig. 7(b). The atomic structure around the APB is not resolved in the STM image, and it is difficult to identify locations of Fe_B cations on the APB, as shown in Fig. 7(b). The Fe_B cations in the region of the APB shown in this figure are depicted for convenience to understand the direction of the shift vector, and they do not necessarily indicate the actual locations of the cations. This type of APB was seldom observed in our STM measurements. In our STM images, the portion of the APBs recognized into this type was about 1%.

3.2.3 Out-of-plane $1/4[101]$ shift

The most frequently observed APBs are those with an out-of-plane shift vector of $1/4[101]$. The STM image shown in Fig. 8(a) suggests that the observed APB should be classified into this type of APB. Fe_B rows are rotated by 90° at the APB with respect to the Fe_B rows in the neighboring domain. Because of the symmetry of B-planes containing this type of APB, two possible atomic arrangements are provided at the surface. The topographic image of this APB makes it possible to assign its atomic arrangements into one of the models of the surface, as shown in Fig. 8(b). In contrast to the previous STM images, the surface structure around the APB is clear. Bright spots observed on the APB could be assigned to Fe_B cations at the center of the APB, as depicted in Fig. 8(b).

Since the atomic configurations of APBs surrounding an antiphase domain are not simple, several types of boundaries consisting of the fundamental APBs that have been discussed so far are observed, as shown in Fig. 8(c). In this image, an APB running along the $[130]$ direction is observed. Carefully looking into the topographic image of the boundary, it can be recognized that this boundary consists of an APBs characterized by the out-of-plane shift vector of $1/4[101]$. Investigating several STM images taken on four different Fe₃O₄ films that were grown under the same experimental conditions, about 61% of identified APBs are categorized into the APB with this type of shift vector.

4. Conclusions

In this paper, we have revealed how APBs are observed on the surfaces of Fe₃O₄ films grown epitaxially on MgO(001) substrates. By comparing simple models of APBs, the

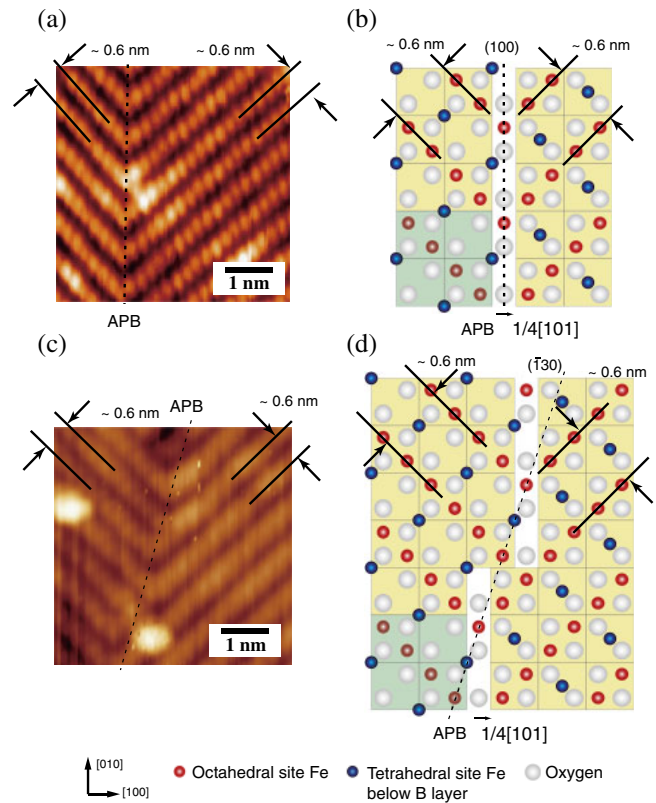


Fig. 8. (Color online) (a) STM image of an APB with a $1/4[101]$ shift. The feedback control set point was $V_S = 2.0$ V, $I = 1$ nA. The scan size was 5×5 nm². The APB is in a (100) plane. (b) Possible surface atomic configuration around an APB with a $1/4[101]$ shift and a (110) boundary plane. (c) STM image of an APB with a $1/4[101]$ shift. The feedback control set point was $V_S = 2.0$ V, $I = 0.3$ nA. The scan size was 5×5 nm². The APB is in a $(\bar{1}30)$ plane. (d) Possible surface atomic configuration around an APB with a $1/4[101]$ shift and a $(\bar{1}30)$ boundary plane.

observed APBs in our experiment are categorized into boundaries with three different phase shift vectors. A reduction in the symmetry of the surface caused by the introduction of APBs gives the surface structures of APBs some variations. The observed APBs in our experiment are classified under the APBs that have been observed by Celotto *et al.* with transmission electron microscopy (TEM).⁶⁾ The tendency of the proportions of each type of APB estimated using our experimental results (ten images of four samples) are nearly the same as that in their report.⁶⁾ In our experiment, the proportion of the APBs with an in-plane $1/4[110]$ shift is about 38% and that of the APBs with an out-of-plane $1/4[101]$ shift is about 61%. Only about 1% of the boundaries are classified into APBs with an in-plane $1/2[100]$ shift. These findings discussed in this paper will be useful for the investigation of local electronic properties or magnetic properties in regions containing well-defined APBs.

Acknowledgments

This work was partially supported by a Grant-in-Aid for Scientific Research S (No. 2222100700) and a grant for the Global COE Program, “Center for Next-Generation Information Technology based on Knowledge Discovery and Knowledge Federation” from the Ministry of Education, Culture, Sports, Science and Technology of Japan.

- 1) A. Yanase and K. Shiratori: *J. Phys. Soc. Jpn.* **53** (1984) 312.
- 2) A. Yanase and N. Hamada: *J. Phys. Soc. Jpn.* **68** (1999) 1607.
- 3) Z. Zhang and S. Satpathy: *Phys. Rev. B* **44** (1991) 13319.
- 4) W. Eerenstein, T. T. M. Palstra, T. Hibma, and S. Celotto: *Phys. Rev. B* **66** (2002) 201101.
- 5) T. Hibma, F. C. Voogt, L. Niesen, P. A. A. van der Heijden, W. J. M. de Jonge, J. J. T. M. Donkers, and P. J. van der Zaag: *J. Appl. Phys.* **85** (1999) 5291.
- 6) S. Celotto, W. Eerenstein, and T. Hibma: *Eur. Phys. J. B* **36** (2003) 271.
- 7) D. T. Margulies, F. T. Parker, M. L. Rudee, F. E. Spada, J. N. Chapman, P. R. Aitchison, and A. E. Berkowitz: *Phys. Rev. Lett.* **79** (1997) 5162.
- 8) R. G. S. Sofin, S. K. Arora, and I. V. Shvets: *Phys. Rev. B* **83** (2011) 134436.
- 9) A. Subagyo, Y. Sasaki, H. Oka, and K. Sueoka: *Phys. Status Solidi B* **244** (2007) 4482.
- 10) A. Subagyo and K. Sueoka: *Jpn. J. Appl. Phys.* **45** (2006) 2255.
- 11) R. W. G. Wyckoff: *Crystal Structures* (Krieger, Malabar, 1982) 2nd ed., Vols. 1–3.
- 12) M. Fonin, R. Pentcheva, Yu. S. Dedkov, M. Sperlich, D. V. Vyalikh, M. Scheffler, U. Rüdiger, and G. Güntherodt: *Phys. Rev. B* **72** (2005) 104436.
- 13) I. V. Shvets, G. Mariotto, K. Jordan, N. Berdunov, R. Kantor, and S. Murphy: *Phys. Rev. B* **70** (2004) 155406.
- 14) B. Stanka, W. Hebenstreit, U. Diebold, and S. A. Chambers: *Surf. Sci.* **448** (2000) 49.
- 15) F. C. Voogt, T. Fujii, P. J. M. Smulders, L. Niesen, M. A. James, and T. Hibma: *Phys. Rev. B* **60** (1999) 11193.
- 16) R. Pentcheva, F. Wendler, H. L. Meyerheim, W. Moritz, N. Jedrecy, and M. Scheffler: *Phys. Rev. Lett.* **94** (2005) 126101.